

Mechanisms for dynamic coronal mass supply via evaporative solar “micro-events”

J.C. Brown^{1,2}, S. Krucker³, M. Güdel^{4,2}, and A.O. Benz²

¹ Department of Physics and Astronomy, University of Glasgow, G128QQ, Scotland, UK (john@astro.gla.ac.uk)

² Swiss Federal Institute of Technology, Institute of Astronomy, ETH-Zentrum, 8092 Zürich, Switzerland (benz@astro.phys.ethz.ch)

³ Space Sciences Laboratory, University of California, Berkeley, CA 94720-7450, USA (krucker@ssl.berkeley.edu)

⁴ Paul Scherrer Institute, 5232 Villigen PSI, Switzerland (guedel@astro.phys.ethz.ch)

Received 7 February 2000 / Accepted 15 May 2000

Abstract. The idea that the corona is at least in part supplied by chromospheric evaporation in loop “micro-events” is quantified in terms of the power requirements of evaporation mechanisms, using recent analyses of data on such events in high temperature EUV lines from the SoHO EIT instrument. Estimates are derived for the pre-event and event values of loop density and temperature and it is shown, using the conductive scaling law, that the event emission measure enhancements are too large to be accounted for solely by enhanced conductive flux from coronal heating. That is, observations demand that supply of coronal mass by evaporation events need a mechanism which enhances upper chromospheric heating and not just conductively driven evaporation. Thus coronal mass supply in transients is inextricably linked to direct chromospheric heating processes. Using parametric models of a chromospheric heating function and of the pre-event chromosphere, an estimate is made of the extra power required to yield the emission measure enhancement of a large event evaporatively. The dependence of the result on just how the EUV solar images are interpreted is emphasised and observational tests are discussed for the case of heating by fast particles. Implications of the results in terms of the global supply of the hot corona and wind mass loss are briefly mentioned.

Key words: plasmas – Sun: chromosphere – Sun: corona – Sun: transition region – Sun: solar wind

1. Introduction

The fundamental problem of how the corona is heated is intimately linked to how its mass (and that lost to the wind) is supplied (cf. Ulmschneider et al. 1991, Fleck et al. 1994, Golub & Pasachoff 1997). In a purely radiative stellar atmosphere, thermodynamics demands that the temperature T should drop with radius, so that the atmospheric density n should decline exponentially at an increasing rate. Thus the upper chromosphere and extended corona (and hence the wind) can only exist if they are nonthermally heated. On the other hand such heating is only possible if there is material there to heat! Thus the

heating and the mass supply problems are inextricably linked. They can be approached from two viewpoints. One is deductive - working out how much power theoretical mechanisms, such as wave or current dissipation, are capable of depositing for likely conditions in the sun’s atmosphere (Ionson 1984, Heyvaerts & Priest 1984, Parker 1988, Title & Schrijver 1999, Beliën et al. 1999, Matthaeus et al. 1999). The second is inductive - applying plasma diagnostic techniques to infer, from XUV/SXR data, what are the actual plasma conditions and heating requirements. Here we consider the latter and, in particular, the extent to which recent high resolution data (Krucker et al. 1997, Benz & Krucker 1998, Berghmans et al. 1999, Schrijver et al. 1999) are consistent with the idea of the corona being at least in part sustained not in a steady spherical state but via localised transient ‘events’ - variously termed micro- or nano-events (or -flares) according to their size. In reality there is a hierarchy of event sizes present and much recent effort (Crosby et al. 1993, Shimizu et al. 1994, Krucker & Benz 1998, Aschwanden et al. 2000a, Parnell & Jupp 2000) has gone into statistical studies of which event sizes dominate the total power and mass supply.

Whatever the detailed temporal and spatial properties of the process creating and heating the corona, its existence depends fundamentally on the radiative instability of optically thin hot plasmas with cosmic abundances at temperatures $T > T_c \approx 0.6\text{--}1.0 \times 10^5$ K (e.g. Cox & Tucker 1969). The plasma volumetric radiative loss rate ($\text{erg cm}^{-3} \text{s}^{-1}$) is $n^2 f_{\text{rad}}(T)$ where f_{rad} peaks around T_c . If the nonthermal energy input (heating) per unit volume in the upper chromosphere scales with density as Cn^b then a balance between it and radiative cooling is only possible at those levels where $Cn^b = n^2 f_{\text{rad}}(T)$ can be achieved. Since $f_{\text{rad}} \leq f_{\text{rad}}(T_c) = f_o$ say, this requires $n \geq (C/f_o)^{1/(2-b)}$. Consequently, since $f_{\text{rad}}(T)$ increases with T at $T \leq T_c$, and since n declines hydrostatically with height in the chromosphere, T increases with height (assuming $b < 2$) and there is a height (where $T = T_c$) above which solely radiative balance of heating is impossible. Above there, the plasma becomes radiatively unstable and heats to much higher (coronal) temperatures limited by backward thermal conduction down the steep T gradient (transition zone) created. Thus the deposition of energy in an initially cool radiative atmosphere

Send offprint requests to: J.C. Brown

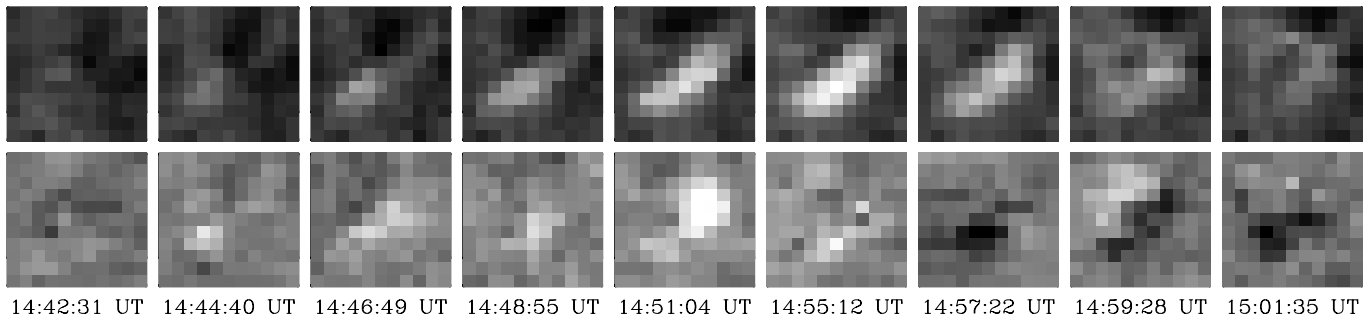


Fig. 1. Time series of a relatively strong enhancement (network flare) of the emission measure between $1\text{--}2 \times 10^6$ K temperature plasma in a quiet Sun region. The emission measure was derived from 171 Å and 195 Å observations by SoHO/EIT. The linear scale of the images is 20700 km. *Top:* images of the coronal emission measure. *Bottom:* difference images of the top row; the previous one is subtracted

results in the heating and ‘evaporation’ of the upper chromospheric ($T \geq T_c$) layers into the hot tenuous coronal state. A full description of the resulting $T(r)$ in the upper layers (corona and transition zone) depends strongly on inclusion of conduction but the height (transition region) of onset of radiative instability depends mainly on the heating function and on $f_{\text{rad}}(T)$. The major enhancement of energy input during solar flares pushes this level deeper into the solar atmosphere, evaporatively enhancing the coronal density. Particle driven flare evaporation was first modelled by Hudson (1972), Brown (1973), Shmeleva & Syrovatskii (1973) but had been pointed out for *any* flare heating process by Sweet (1969), though the term ‘evaporation’ was first used by Antiochos & Sturrock (1978). This dependence of coronal density on evaporative heating rate is central to the remainder of the present paper. (The wider relevance of fast particles in cosmic heating processes was recently discussed by Hirth & Krueger 2000).

Data on the quiet corona of ever better spatial, temporal and spectral resolution have led to the increasing recognition that even the quiet coronal structure is highly inhomogeneous and transient. They have also recently enabled some modelling of physical conditions (Krucker et al. 1997, Benz & Krucker 1999, Krucker & Benz 1998) in the transient events, and of their statistical properties (Benz & Krucker 1998, Krucker & Benz 1998, Berghmans et al. 1999, Parnell & Jupp 2000, Aschwanden et al. 2000b) and their possible role in the global coronal heating (Gold 1964, Priest 1981, Parker 1983). In particular, using high resolution SoHO EIT data, Benz & Krucker (1998) have estimated, pixel by pixel, the time variations of emission measures and temperatures, used these to estimate event densities, masses, and energies, and investigated many of their statistical properties. In this paper we take their results further by considering their physical implications for the evaporation processes, and also discuss line of sight ambiguities of data interpretation which affect the results.

2. Geometric interpretation of event data

Benz & Krucker (1998) (hereafter BK) discuss the evolution of one of the largest local transient micro-events they observed in SoHO EIT data on the ‘quiet’ atmosphere - near disk centre on

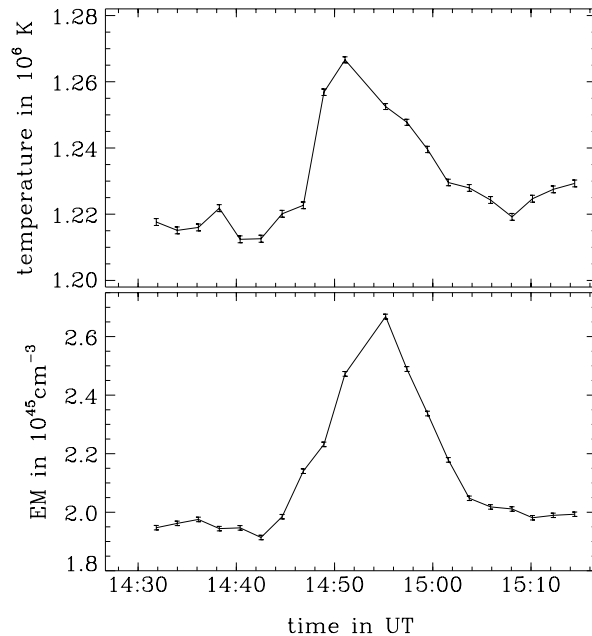


Fig. 2. The time profiles of the event shown in Fig. 1. *Top:* average temperature (formal value) over the area of enhanced intensity; no background was subtracted (cf. Case II). *Bottom:* total emission measure of the same area in the $1\text{--}2 \times 10^6$ K temperature range

July 12 1996 around 14:40–15:00 UT - see Figs. 1 and 2 (taken from BK). We will focus our modelling on it as an example of a micro-event (though recognising that it is exceptionally large) since it was well observed - and so suited to testing theoretical ideas about the evaporation process. We will, however, use data on other events in statistical considerations.

Observations covered a field $7'$ square with a resolution of $2.6'' \approx 1900$ km and a time resolution ≈ 128 s. Pixel fluxes in bands around 171 and 195 Å provided temperature diagnostics in the $1\text{--}2 \times 10^6$ K range. The field evolved from being of roughly uniform brightness to exhibiting an elongated patch of enhanced flux, lasting about 600 s, against a near constant background emission (Fig. 1). If this patch is interpreted as emission from a vertical semicircular loop seen in projection then the toroidal radius $R \approx 7000$ km, the poloidal radius

$a \approx 1500$ km, and the total length and volume are respectively $L = \pi R \approx 22,000$ km, $V = \pi^2 R a^2 \approx 1.55 \times 10^{26}$ cm³ while the projected area of the source $S \approx 4Ra \approx 4.2 \times 10^{17}$ cm² and the loop cross-section is $A = \pi a^2 = 7.1 \times 10^{16}$ cm². Using the fluxes from S in the 171 and 195 Å bands, BK derived the evolution of the emission measure EM_{tot} and mean temperature T_{otot} of the total source volume above area S as a function of time, shown in Fig. 2. (NOTE - we will use T_o to denote temperatures of hot coronal sources, assumed uniform in each source, reserving $T(N)$ for the depth dependent chromospheric temperature when we come to model the chromospheric evaporation). T_{otot} was found to rise from 1.22×10^6 K to a peak $\approx 1.27 \times 10^6$ K over about 200 s with EM_{tot} rising from 1.9×10^{45} cm⁻³ to a (slightly later) peak of 2.7×10^{45} cm⁻³, both then declining over a similar timescale.

To study mechanisms what we want is not the evolution of EM, T_o for the whole projected volume but of the values in the loop itself. These can only be derived from the line of sight projected data by making prior assumptions concerning what fraction - say ϕ - the pre-event loop emission measure contributes to the observed total flux (loop and background). Since the results turn out to be sensitive to the assumptions made, we consider two limiting cases, namely where ϕ approaches 0 and 1. In both we assume that the background values of EM_{tot}, T_o do not change during the event and that the pre-event loop temperature is the same as the background - namely $T_{o1} \approx 1.22 \times 10^6$ K - consistent with the relative constancy of the pixels outside the event area and with the uniformity of the pre-event field of view. Since the isothermal density scale height at the pre-event temperature T_{o1} is $H_o = 2kT_{o1}/m_p g \approx 7 \times 10^9$ cm is much larger than the loop height R , the density in the loop should be spatially quite uniform under hydrostatic conditions. Secondly, since the sound travel time up the loop $\approx R/(kT_o/m_p)^{1/2} \approx 70$ s is shorter than the event duration, the loop can be approximated as evolving through a series of hydrostatic states.

Case I

The interpretation given to the data by BK is that the pre-event loop contribution to the observed fluxes is negligibly small - i.e. $\phi \rightarrow 0$ - because the loop volume is small. Then the rise in EM can be thought of in terms of the filling of an essentially empty loop by hot evaporated material. Under this assumption, and those mentioned above, subtraction of the mean pre-event photon fluxes from the fluxes during the event yields the flux evolution for the loop alone. If we denote pre-event and peak event values by subscripts _{1,2} then for the loop $EM_1 = 0$ in this case, so

$$\begin{aligned} EM_2 &= EM_{\text{tot}2} - EM_{\text{tot}1} = (2.7-1.9) \times 10^{45} \text{ cm}^{-3} \\ &= 8.0 \times 10^{44} \text{ cm}^{-3} \end{aligned} \quad (1)$$

which, for loop volume $V = 1.5 \times 10^{26}$ cm³ gives peak event values for the following loop parameters - density $n_{o2} = \sqrt{EM_2/V}$, total protons in (and injected into) the loop \mathcal{N}_2 , total injected mass $\mathcal{M}_2 = \mathcal{N}_2 m_p$, namely

$$\begin{aligned} n_{o2} &= 2.27 \times 10^9 \text{ cm}^{-3}; \mathcal{N}_2 = 3.52 \times 10^{35} \\ \mathcal{M}_2 &= 5.90 \times 10^{11} \text{ g} \end{aligned} \quad (2)$$

The temperature T_{o2} of the loop at event peak, inferred from the spectral fluxes with the pre-event background values subtracted, is considerably higher than the source area mean peak temperature (1.27×10^6 K) inferred from the total fluxes since the loop volume is small. Its value, and the corresponding peak loop top pressure $P_{o2} = 2n_{o2}kT_{o2}$ are

$$T_{o2} \approx 1.44 \times 10^6 \text{ K}; P_{o2} \approx 0.90 \text{ dyne cm}^{-2} \quad (3)$$

while the corresponding thermal and gravitational energies of the injected matter are

$$\begin{aligned} \mathcal{E}_t &= 3\mathcal{N}kT_o \approx 2.10 \times 10^{26} \text{ erg} \\ \mathcal{E}_g &= \mathcal{N}m_p g R \approx 1.13 \times 10^{25} \text{ erg.} \end{aligned} \quad (4)$$

(These values correct a discrepancy between the EM values in BK Fig. 2 and in their text, the latter being incorrect).

A key variable in some of our hydrostatic evaporation modelling proves to be the *vertical* plasma column density N downward from the loop top. At the base of the hot loop (or top of the chromosphere where the radiative instability temperature T_c is reached) this takes a value $N_{c2} = \mathcal{N}_2/\pi^2 a^2$. At event peak this is

$$N_{c2} = 1.59 \times 10^{18} \text{ cm}^{-2} \quad (5)$$

However the pre-event values of N_{c1}, n_{o1} are also relevant in relation to underlying chromospheric conditions and how these affect evaporation. In the BK assumption N_{c1}, n_{o1} are approximated by zero but the pre-event loop cannot be truly empty. If it were, the finite pressure of the underlying chromosphere would fill the loop with material which, as its density fell, would become radiatively unstable to any ambient heating and rise to coronal temperatures. (This is the essence of the conductive loop scaling law - Rosner et al. 1978 - cf. Sect. 3.2. The loop density and temperature adjust by evaporation until in pressure and energy balance with the chromosphere). A more reasonable a priori physical assumption is that the pre-event loop density n_{o1} is not zero but the same as that of the local embedding background material. If we take the density of the loop as uniform and that of the extended background as having an exponential height distribution with scale height H_o then the ratio of pre-event emission measure EM_1 in the loop to the total is $\phi \approx \pi^2 a/2H_o \approx 0.1$ so the pre-event loop contribution to EM_{tot} should indeed be quite small and the BK approximation of neglecting it in their spectral analysis reasonably good. However, to estimate the finite pre-event loop values of N_{c1}, n_{o1} which determine respectively the weight and top pressure of hot matter in the loop which the chromospheric top pressure must balance, we therefore replace the BK zero values with those implied by the above emission measure fraction $\phi \approx 0.1$. Namely we set $EM_1 = \phi EM_{\text{tot}1} \approx 1.9 \times 10^{44} \text{ cm}^{-3} = n_{o1}^2 V = \pi^2 a^2 N_{c1}^2/R$ which yields values

$$n_{o1} = 1.06 \times 10^9 \text{ cm}^{-3}; N_{c1} = 7.83 \times 10^{17} \text{ cm}^{-2} \quad (6)$$

and the corresponding pre-event loop top pressure $P_{o1} = 2n_{o1}kT_{o1}$ is

$$P_{o1} = 0.37 \text{ dyne cm}^{-2} \quad (7)$$

Case II

The assumption at the other extreme from $\phi = 0$ is that $\phi = 1$ - i.e. ALL of the emission seen in the event area originates in the loop both before and during the event. To make the pre-event field of view look uniform, this would require a rather fortuitous distribution of background density - but is not precluded by the data and puts opposite bounds on parameters from Case I. Then all of the observational data in the projected event area refer solely to the loop volume and we get the following results, which differ notably from Case I

$$T_{o2} = 1.27 \times 10^6 \text{ K (and } T_{o1} = 1.22 \times 10^6 \text{ K)} \quad (8)$$

(a much smaller temperature rise than in Case I)

$$\begin{aligned} n_{o1} &= \sqrt{EM_{\text{tot}1}/V} \approx 3.50 \times 10^9 \text{ cm}^{-3} \\ n_{o2} &= \sqrt{EM_{\text{tot}2}/V} \approx 4.17 \times 10^9 \text{ cm}^{-3} \end{aligned} \quad (9)$$

with

$$\begin{aligned} \Delta\mathcal{N} &= \mathcal{N}_2 - \mathcal{N}_1 = V(n_{o2} - n_{o1}) = 1.04 \times 10^{35} \\ \Delta\mathcal{M} &= \mathcal{M}_2 - \mathcal{M}_1 = 1.75 \times 10^{11} \text{ g} \end{aligned} \quad (10)$$

with corresponding energy contents of injected matter

$$\mathcal{E}_t \approx 5.49 \times 10^{25} \text{ erg}; \quad \mathcal{E}_g \approx 3.35 \times 10^{24} \text{ erg} \quad (11)$$

all of which are lower than in Case I because the pre-existing material in the loop reduces the amount to be added to reach the peak emission measure. The corresponding values of loop vertical column density N_c and of top pressure P_o are

$$N_{c1} \approx 2.45 \times 10^{18} \text{ cm}^{-2}; \quad N_{c2} \approx 2.92 \times 10^{18} \text{ cm}^{-2} \quad (12)$$

$$P_{o1} \approx 1.18 \text{ dyne cm}^{-2}; \quad P_{o2} \approx 1.46 \text{ dyne cm}^{-2} \quad (13)$$

Among the most important of the above results, which will be used below in our discussion of evaporation models, are the large differences in the inferred model parameters between the two Cases with distinct source geometry assumptions. In particular the fractional enhancements of coronal temperature and column density are respectively for Case I

$$\Delta T_o/T_o \approx 0.17 \text{ and } \Delta N_c/N_c \approx 1.05, \quad N_{c2}/N_{c1} = 2.05$$

and for Case II

$$\Delta T_o/T_o \approx 0.04 \text{ and } \Delta N_c/N_c \approx 0.19, \quad N_{c2}/N_{c1} = 1.19$$

We will see that the difference between these N_{c2}/N_{c1} values substantially affects the power input required to drive the event by evaporation. In either interpretation, the fractional rises in N_c are much larger than in T_o and to that extent the events could perhaps be thought of more as “chromospheric evaporation micro-events” than as “coronal heating micro-events” but

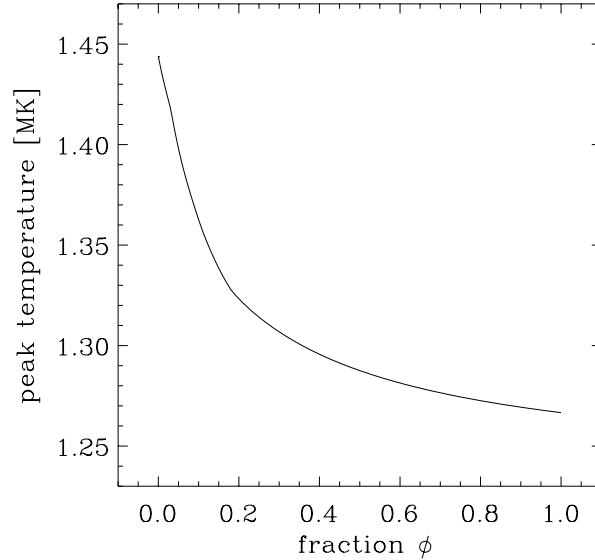


Fig. 3. Plot of inferred peak loop temperature versus the assumed fraction ϕ of the observed photon flux arising from within the loop

the importance of the coronal heating needs to be assessed in relation to conductive evaporation. This dependence on geometric interpretation affects the relative importance of thermal conduction versus other evaporation mechanisms as we discuss in the next section. To emphasise the dependence of physical parameters on the geometric interpretation we have calculated the peak loop temperature as a function of ϕ , the fraction of the projected loop area pre-event flux contributed by the loop itself - i.e. by subtracting off a fraction $1 - \phi$ of the preflare fluxes in deriving the peak loop temperature, with the results shown in Fig. 3.

3. Drivers for evaporation events

3.1. General points

We first note that loop EM enhancements need not necessarily involve injection of extra matter (nV), but might occur by compression since $EM = n \times nV$ but such compression could also heat the gas. An adiabatic compression, of a fixed mass $\propto nV$, enhancing EM by a factor of ≥ 4 , as required in Case I above, in the absence of any cooling would enhance T_o by a factor ≥ 2.5 while enhancing EM by a factor of 1.42, as required in Case II above, would increase T_o by a factor of 1.26. In both Cases these temperature rises are well in excess of those inferred from the corresponding interpretation of the data. This argues against a compressive model, provided cooling effects during the compression are not large. This will only be the case if the compression time is short compared to the cooling time. In fact the estimated radiative cooling time and the event rise time are roughly comparable so that the enhanced density might result in a fall rather than a rise in T_o . Such temperature drops are observed in a few events so models based on compression as the source of EM increase are worth pursuing using a time dependent treatment of the heating and cooling processes. Here,

however, we will concentrate on models for interpretation of the events as evaporative. (Certainly some evaporation must occur to replenish the wind mass loss and to explain the blue shifts sometimes detected). We also observe that a lower limit to the energy flux needed for such enhanced evaporation is simply the value of $F_{\mathcal{E}} = (\mathcal{E}_t + \mathcal{E}_g)/(\pi a^2 \Delta t)$ where $\Delta t \approx 300$ s is the effective event duration. This gives $F_{\mathcal{E}} \approx 10^7$ erg cm⁻² s⁻¹ for the Case I interpretation and $F_{\mathcal{E}} \approx 3 \times 10^6$ erg cm⁻² s⁻¹ for Case II. These are both underestimates in that we have neglected the work done by expansion of the evaporating gas (which will be comparable to \mathcal{E}_t) and, more importantly, the energy input required to cause evaporation of ΔN chromospheric particles per unit area by heating them enough to offset the strong radiative losses at $T \leq T_c$. We can get a rough estimate of the latter by noting that the radiative flux at $T \approx T_c$ from a 1 cm² column of mean density \bar{n} and column density ΔN is $F_{\text{rad}} \approx \Delta N \bar{n} f_o \approx 5 \times 10^6$ erg cm⁻² s⁻¹ $\times (\bar{n}/10^{10}$ cm⁻³) for $\Delta N \approx 8.2 \times 10^{17}$ cm⁻². We will see in Sect. 2.2 that the density at the top of the pre-event chromosphere is well in excess of 10^{10} cm⁻³ so that the radiative losses are important compared with $F_{\mathcal{E}}$. On the other hand we have thus far ignored the contribution of the pre-event chromospheric heating which maintains the mean ambient upper chromosphere. In the remainder of this paper we therefore formulate a model of energy balance in a heating event, taking account of this ambient heating.

3.2. Conductive evaporation

The energy balance of hydrostatic loops dominated by thermal conduction and radiation for a wide class of heating mechanisms operating in the corona was discussed extensively by Rosner et al. (RVT) (1978) and many subsequent authors. The essence of their results is, as already mentioned, governed by a scaling law which links conductive flux created by the high loop top temperature T_o (itself generated by some coronal heating mechanism) and length L to the loop density n_o by the requirement of hydrostatic pressure balance with the top of the chromosphere. The basic RVT scaling law for a loop of top temperature $T_o(K)$, density $n_o(\text{cm}^{-3}) = 10^9 n_9$ and total length $L(\text{cm}) = 10^9 L_9$ ($L = \pi R$ for a semicircular loop) can be written

$$n_9 = 2.6 \frac{T_6^2}{L_9} \quad (14)$$

which, for a loop of cross sectional area $A = \pi a^2 = 10^{16} A_{16}$ cm², implies a relation between emission measure and T , viz

$$EM(\text{cm}^{-3}) = 6.76 \times 10^{43} \frac{A_{16} T_6^4}{L_9} \quad (15)$$

For the loop dimensions given in Sect. 2 for the BK event, this expression predicts an emission measure of 4.8×10^{44} cm⁻³ for the pre-event loop, assuming a temperature of 1.22×10^6 K, which lies between our observational estimates of 1.9×10^{44} cm⁻³ for our Case I interpretation and with 1.9×10^{45} cm⁻³ for our Case II interpretation. Given the uncertainties of the geometry, this suggests the pre-event loop is

near the RTV scaling law conditions of conductive and pressure equilibrium.

If the loop evolution in the event were dominated by conduction in a series of hydrostatic states, then we would expect it to follow Eq. (15) which, for fixed loop geometry, can be expressed as

$$\frac{EM_2}{EM_1} = \left[\frac{T_{o2}}{T_{o1}} \right]^4 \quad (16)$$

For the parameters of interpretative Case I the loop temperature rise $\times 1.44/1.22$ should produce a conductive rise in emission measure by a factor $\times 1.94$ as compared with the factor $8/1.9 = \times 4.21$ inferred from the data in this Case. For Case II parameters, from $T_{o2}/T_{o1} = 1.27/1.22 = 1.04$ we would predict a rise $EM_2/EM_1 = \times 1.17$ as compared with the observed value $EM_2/EM_1 = 2.7/1.9 = 1.42$ for that Case. Thus, in neither interpretation, is the hot loop temperature rise nearly enough to drive the required evaporative increase in loop emission measure during the event. Thus while conduction must play some role in loop event energy transport it cannot be the dominant driver of evaporation during the peak of the event, at least in a quasi-steady regime. Physically, if we estimate the conductive energy flux available by $F_{\text{cond}} \approx (2/7) \kappa_o T^{7/2}/(L/2)$ then we find, for the BK event L , $F_{\text{cond}} \approx 2.5 \times 10^5 (T_{o2}/10^6)^{7/2}$ which gives $\approx 10^6$ erg cm⁻² s⁻¹ for Case I and 0.6×10^6 erg cm⁻² s⁻¹ for Case II. These values fall short, by over one order of magnitude, of our later estimates (Sect. 3.5) of the flux needed to yield the amounts of BK event evaporation inferred from the data. (This estimate of F_{cond} may be too low if T_o extends so near the transition zone that the temperature gradient length is $\ll L/2$. On the other hand, it does not allow for energy lost by radiation along the conduction path from T_o to T_c .) We therefore require a driver for the event evaporation which penetrates the upper chromosphere to deeper layers than the conductive flux enhancement generated by the relatively small observed rises in hot loop temperature. Of course, once the additional heating ends, the loop should return to an RTV conductive state, with the extra hot matter condensing back into the chromosphere.

As well as examining this one event we can look at what the statistics of event parameters tell us about the relevance of conductive scaling law (15) to the energetics of the evaporation mechanism involved. Events differ in geometrical size and for many small events it is hard to estimate L, A accurately even if the evolution of EM, T_o from the loop as a whole is determined. We have therefore selected a set of events and used the number of pixels (i.e. total projected area $S = 4aL/\pi$) they occupy to estimate $L, a, A = \pi a^2$ (and also ϕ for Case I) by assuming that on average events have the same L/a as the large BK event namely $L/a \approx 14.7$. We then have estimates of the pre-event and event EM, T_o values and (with A, L scaled out in the fractional changes) we can plot $\Delta EM/EM$ versus $\Delta T_o/T_o$ with the results shown in Figs. 4 and 5 for Cases I and II respectively. (The BK event is indicated in the figures). These data results show no resemblance to the scaling law prediction (16) confirming that thermal conduction is not the main controlling

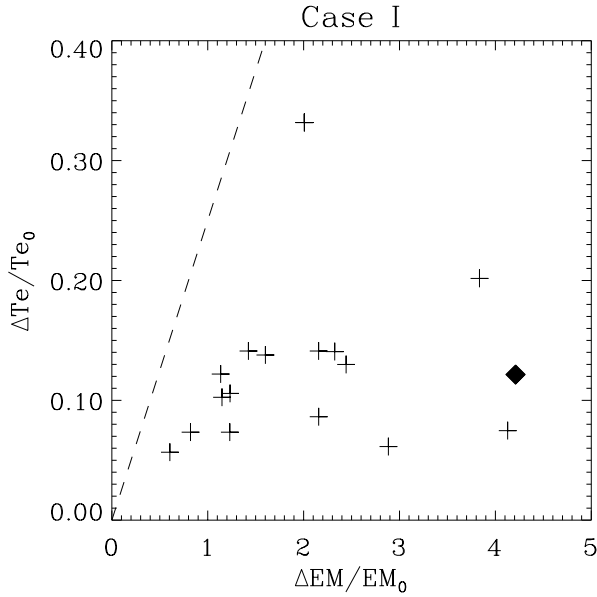


Fig. 4. Plot of the fractional temperature increase versus the fractional emission measure increase for our set of observed events (The large BK event is indicated by a solid diamond). The dashed line is the expected relationship for conduction dominated loops (RVT). This is for the case where background fluxes have been subtracted to get the loop emission, using $\phi = 0.1$, relevant to Case I in the text

factor in event evaporation. (We tried an alternative assumption $L/a \approx 4$, perhaps more apt for smaller squatter loops. Though this changed the values of $\Delta EM/EM$ and ϕ , we still found no resemblance to prediction (16)). In Sect. 3 we will examine parametric models involving more penetrating forms of evaporative energy flux. To keep the analysis simple, in treating these we will neglect the effects of conduction. While conduction is certainly crucial in determining the temperature profile in the upper loop transition zone where the temperature gradient is steep and the conductivity is high, we will be considering lower temperatures (at and below T_c) at the base of the loop transition zone where radiative instability is reached under the effects of event energy input, resulting in the evaporation event. The ambient heating and the additional heating required for an event depend on the pre-event chromospheric, $n(N), T(N)$ structure and we first derive a parametric representation of this structure.

3.3. Pre-event chromosphere structure models

We will describe the magnitude of evaporation events by comparing the pre-event and event values of the *vertical* column densities N_{c1}, N_{c2} of loop particles lying above the base of the transition zone (top of the chromosphere) located at $T = T_c$. Material above that is taken to expand to uniform density in the hot coronal loop. Both chromospheric loop states are taken to be in hydrostatic and energy equilibrium, the latter being a balance between the sum of event and ambient heating rates per unit volume, which we will write respectively as $n(N)H_E(N), n(N)H_A(N)$, and optically thin radiative losses $n^2(N)f_{\text{rad}}(T(N))$ where N is the total *vertical* column density

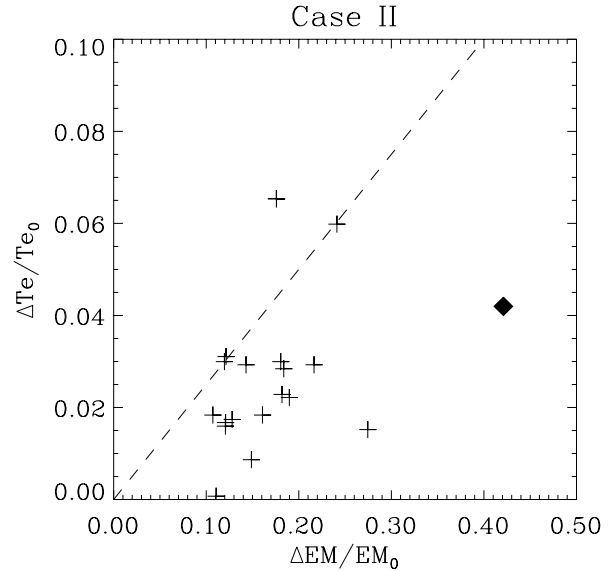


Fig. 5. Plot of the fractional temperature increase versus the fractional emission measure increase for our set of observed events (The large BK event is indicated by a solid diamond). The dashed line is the expected relationship for conduction dominated loops (RVT). This is for the case where no background fluxes have been subtracted to get the loop emission, loop emission being assumed to dominate i.e. assuming $\phi = 1$, Case II in the text.

from the loop top down to the point in question and $n(N), T(N)$ are the density and temperature there. (Since we are dealing mainly with the upper chromosphere we assume full ionisation.) For the radiative loss function in $T \leq T_c$ we use the approximation of Craig & McClymont (1978) viz

$$f_{\text{rad}}(T) = f_o \left(\frac{T}{T_c} \right)^3 \quad (17)$$

where $f_o \approx 6 \times 10^{-22} \text{ erg cm}^3 \text{ s}^{-1}$ for $T_c = 6 \times 10^4 \text{ K}$ which we will adopt here. (The value of T_c is somewhat higher for calculations with different atomic coefficients and abundances but the form of our analysis will be unchanged). $n_1(N), T_1(N)$ and $n_2(N), T_2(N)$ will respectively describe the structures of the pre-event and event chromosphere models for which we will also specify (from data) the pre-event and event loop top pressures P_{o1}, P_{o2} . Hydrostatic equilibrium relates $n(N), T(N)$ for each structure by

$$n_{1,2}(N) = \frac{P_{o1,2} + m_p g N}{2kT_{1,2}(N)} \quad (18)$$

To complete the description of the pre-event atmosphere by specifying $T_1(N)$ we will use the empirical parametric form

$$T_1(N) = T_c \times \exp \left[a \left(\left(\frac{N_c}{N} \right)^\alpha - 1 \right) \right] \quad (19)$$

with dimensionless parameters a, α chosen to fit standard detailed models of the quiet chromosphere. This is designed to reach a low $T \approx 6000 \text{ K}$ plateau at large N and to rise very steeply as $N \rightarrow N_c$. We have found that this form can give a

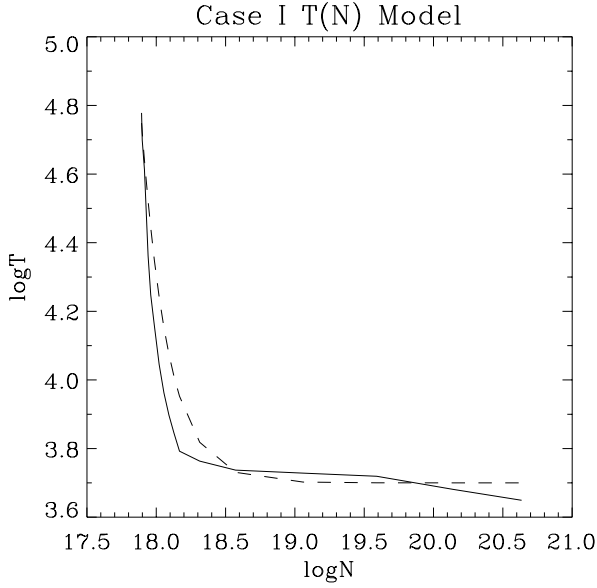


Fig. 6. Pre-event chromospheric temperature model $T(N)$ for Case I low density pre-event loop structure

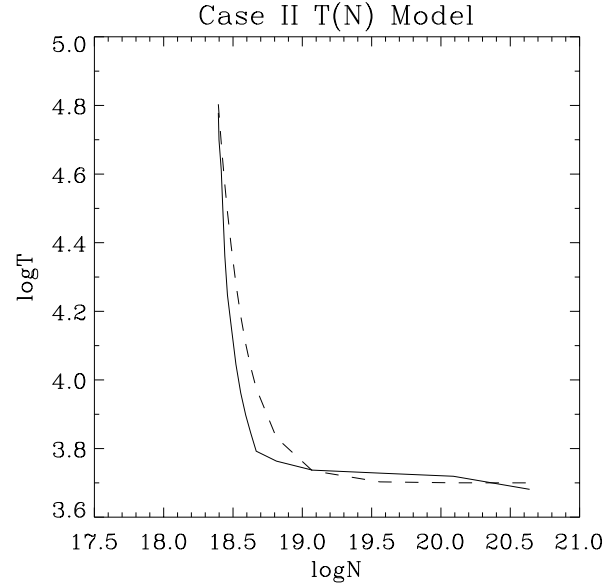


Fig. 7. Pre-event chromospheric temperature model $T(N)$ for Case II high density pre-event loop structure

reasonably good fit to $T(N)$ in $6 \times 10^3 - 6 \times 10^4$ K for a wide range of models, including the four models of Fontenla et al. (1991) with different top pressures and also the active region model of Basri et al. (1978). For the inferred model values we had $N_{c1} = 7.83 \times 10^{17} \text{ cm}^{-2}$, $n_{o1} = 1.06 \times 10^9 \text{ cm}^{-3}$ for Case I and $N_{c1} = 2.48 \times 10^{18} \text{ cm}^{-2}$, $n_{o1} = 3.50 \times 10^9 \text{ cm}^{-3}$ for Case II. With the pre-event loop top temperature $T_o \approx 1.22 \times 10^6$ K by Eq. (1) the pre-event pressure at the top of the chromosphere where $T_1 = T_c$, $n = n_{c1}$ has to be such that

$$n_{c1} = \frac{2n_{o1}KT_o + N_{c1}m_p g}{2kT_c} \quad (20)$$

giving $n_{c1} = 2.7 \times 10^{10} \text{ cm}^{-3}$ for Case I and $= 7.8 \times 10^{10} \text{ cm}^{-3}$ for Case II. (We note that $2n_{o1}kT_o/N_{c1}m_p g \approx 10$ in both Cases which shows that the top pressure is a major factor in determining the chromospheric density. This emphasises the fact that we cannot neglect the material in the pre-event loop in considering the physics). We have chosen to adopt for our present models of $T_1(N)$ the Basri model with scaled down values of the top pressure to match the values of N_{c1} estimated for the BK event in Cases I and II. These scaled Basri models of $T(N)$ are shown in Figs. 6 and 7 along with the fitted form Eq. (19) with values $a = 2.422$, $\alpha = 2.260$ for Case I and $a = 2.528$, $\alpha = 2.202$ for Case II.

3.4. A parametric heating model for evaporation events

We will treat the micro-event evaporation problem in a similar way to Brown’s (1973) flare modelling but with the following generalisations: (a) We include a finite and changing loop top pressure - this acts to reduce evaporation and so to increase power requirements since it raises chromospheric density; (b) Our parametric heating functions is intended to describe a wider range of heating mechanisms than just particle beams though

we discuss these later; (c) We emphasise the ambient chromospheric heating term - this was small in Brown’s (1973) calculations for large flare heating rates. This term substantially reduces the *additional* heating flux needed to produce micro-event evaporation, though it has to be included in the global energy budget.

Given these assumptions, the steady energy equation for the event state chromosphere can now be written

$$n_2(N)(H_A(N) + H_E(N)) = n^2(N)f_{\text{rad}}(T(N)) \quad (21)$$

where the heating nH per unit volume is assumed, following Brown (1973), to scale as $n(N)$ when $n(N)$ changes. The value of the ambient heating is obtained by requiring that it match the radiative losses in the pre-event chromosphere, i.e.

$$H_A(N) = n_1(N)f_{\text{rad}}(T_1(N)) \quad (22)$$

Substituting for $H_A(N)$, $n_{1,2}(N)$, $T_1(N)$ and form (17) for $f_{\text{rad}}(T)$ we then get for the event $T(N)$ the equation

$$\left[\frac{P_{o2}}{2kT_c} + \frac{N}{\ell} \right] \left[\frac{T_2(N)}{T_c} \right]^2 - \left[\frac{P_{o1}}{2kT_c} + \frac{N}{\ell} \right] \times \exp \left[2a \left(\left(\frac{N_{c1}}{N} \right)^\alpha - 1 \right) \right] = \frac{H_E(N)}{f_o} \quad (23)$$

where $\ell = 2kT_c/m_p g = 3.7 \times 10^8$ cm is the isothermal scale height at temperature T_c . Since we are considering a situation in which the coronal loop T_o , L values change very little the loop top pressures P_{o1} , P_{o2} are related by

$$P_{o2} = P_{o1} \frac{N_{c2}}{N_{c1}} \quad (24)$$

Solution of (23) with (24) for each N with an assumed form for $H_E(N)$ and values for atmospheric parameters P_{o1} , a , α , N_{c1}

would yield $T_2(N)$. Here, however, we are mainly interested in determining the amount of evaporation in terms of N_{c2} such that $T_2(N_{c2}) = T_c$. Defining $x = N_{c2}/N_{c1} \geq 1$ as the evaporation enhancement ratio, and dimensionless pressure parameter p and heating function $h(x)$ as

$$p = \frac{P_{o1}\ell}{2N_{c1}kT_c} = \frac{P_{o1}}{N_{c1}m_p g} \quad (25)$$

$$h(x) = \frac{\ell H_E(N)}{(1+p)f_o N_{c1}} \quad (26)$$

then Eq. (23) with $T_2 = T_c$ gives the equation for x

$$x - \frac{x+p}{1+p} \times \exp[-2a(1-x^{-\alpha})] = h(x) \quad (27)$$

to be solved for evaporation enhancement factor x once $h(x)$ is specified, as follows.

We parametrise the variation of heating rate $H_E(N)$ with depth as $\propto (N/N_{c1})^{-\beta}$ where $\beta \geq 1$ which, with the normalisation $\int_{N_{c1}}^{\infty} H_E(N)dN = F_{c1}$ to the total heating flux F_{c1} below N_{c1} leads to

$$H_E(N) = (\beta - 1) \frac{F_{c1}}{N_{c1}} \left(\frac{N}{N_{c1}} \right)^{-\beta} \quad (28)$$

for which the dimensionless equivalent is

$$h(x) = h_o x^{-\beta} \quad (29)$$

where

$$h_o = \frac{\beta - 1}{p + 1} \frac{\ell F_{c1}}{f_o N_{c1}^2} \quad (30)$$

and Eq. (27) for x becomes

$$x - \frac{x+p}{1+p} \times \exp[-2a(1-x^{-\alpha})] = h_o x^{-\beta} \quad (31)$$

(We also considered the case with $\beta = -1$ and with heating cut off at a finite depth. This is such that the volumetric heating rate scales roughly as n^2 since $N \propto n$ for constant T . Thus the ratio of heating to radiation n is essentially constant over the heated volume and the event heating effect is constant there. Results were very similar to those for β near 1.0 with the same total heating flux, so we do not present them here).

3.5. Results

For any given pre-event atmosphere parameters (a, α, N_{c1}) Eqs. (27) and (31) could be used in two ways. Firstly we can solve them for the value of the relative transition zone column density $x = N_{c2}/N_{c1}$ for a given energy flux F_{c1} and heating depth distribution parameter β , or we can use them to find the energy flux F_{c1} needed to produce a specified amount of evaporation x for a given initial atmosphere and depth distribution parameter. For the BK event parameters given above we will follow the latter approach. For our pre-event atmospheric parameters we take the numerical values for a, α, N_{c1} given above

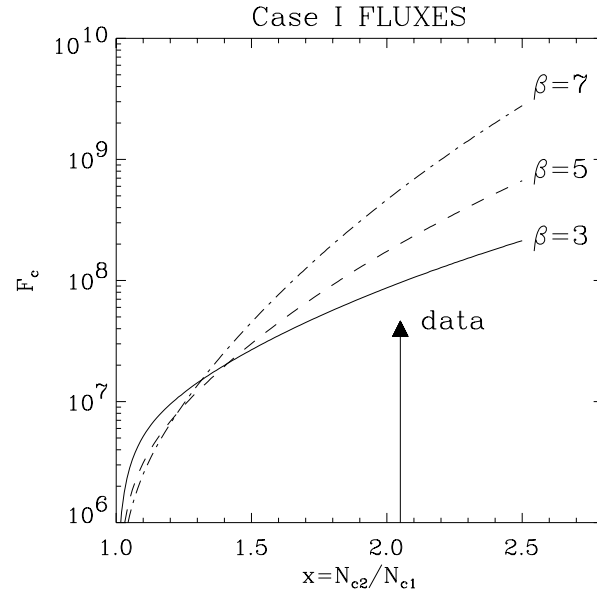


Fig. 8. Energy flux F_{c1} required for evaporative enhancement of coronal column density by a factor x for the pre-event chromospheric model appropriate to low density pre-event loop model of Case I in the text

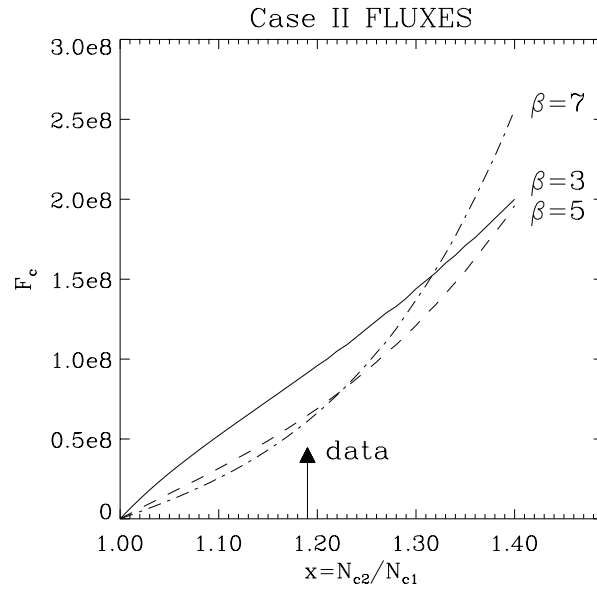


Fig. 9. Energy flux F_{c1} required for evaporative enhancement of coronal column density by a factor x for pre-event chromospheric model appropriate to high density loop model of Case II in the text

and $p \approx 10.5$ in both cases. Using these in energy Eq. (27), we find the results shown in Figs. 8, 9 for $F_{c1}(x)$ for various β . The values $x_o = 2.05, 1.19$ inferred from the BK event data for the two Cases of interpretation are shown as arrows on Figs. 8 and 9.

We see that Case I needs a much larger energy flux $F_c = 10^8 - 10^9 \text{ erg cm}^{-2} \text{ s}^{-1}$ (especially for large β) than Case II $F_c \approx 5 - 8 \times 10^7 \text{ erg cm}^{-2} \text{ s}^{-1}$ to drive enough extra evaporation to explain the EM data. The former in fact approaches the flux involved in small flares (Brown 1973). This is because

Case I needs 3.4 times as much evaporated mass as Case II and because the evaporated mass does not simply scale linearly with F_c unless $x - 1 \ll 1$. Note that both values are well in excess of the available conductive flux F_{cond} estimated in Sect. 3.2. If we estimate the conductive heating rate H_{cond} per particle by $H_{\text{cond}} \approx F_{\text{cond}}/(n_o L/2)$ and the event heating rate by $H_E \approx F_{c1}/N_{c1}$ (Eq. 28) then $H_{\text{cond}}/H_E \approx 2 \times (F_{\text{cond}}/F_{c1})$ since $n_o \approx N_{c1}/L$. The observational estimate of F_{cond}/F_{c1} is $\ll 1$ implying that $H_{\text{cond}}/H_E \ll 1$ consistent with our neglect of conductive heating in our modelling.

The scaling of F_c with evaporated mass $\Delta N \propto (x - 1)N_{c1}$ can be seen analytically from (27) in the limits of large and small $x - 1$. For $x \gg 1$ and taking $e^{-2a}/(1 + p) \ll 1$ we find

$$x = \frac{N_{c2}}{N_{c1}} \rightarrow \left[\frac{(\beta - 1)\ell F_{c1}}{(p + 1)f_o N_{c1}^2} \right]^{\frac{1}{p+1}} \quad (32)$$

which is the same as Brown (1973) found for intense flare evaporation by an electron beam of spectral index $\delta = 2\beta - 1$. For $\delta = 5, \beta = 3$, x only increases as $F_c^{0.25}$. This means that *per unit energy flux* we get more evaporation for small than for large heating fluxes. Consequently more evaporation would be produced for a specified total heating power by spreading it over a larger area than concentrating it in a small area. Physically this is because ‘digging’ deeper into the chromosphere demands rapidly increasing energy flux to offset the increase in radiative losses with $n(N)$ and to drive $T > T_c$.

We can also obtain the analytic relation between F_c and x for small amounts of evaporation $\epsilon = x - 1 \ll 1$. In this limit (for $p \gg 1$) (27) then gives

$$\epsilon \rightarrow \frac{\beta - 1}{(p + 1)(1 + 2a\alpha)} \frac{\ell F_{c1}}{f_o N_{c1}^2} \quad (33)$$

which, unlike (32) is linear in F_c .

For example, if we adopt the Case II interpretation of the BK event, and take $\beta \approx 2$ then numerically (33) becomes

$$\Delta N_c = \epsilon N_{c1} = 3 \times 10^{16} \text{ cm}^{-2} [F_{c1}/10^7 \text{ erg cm}^{-2} \text{ s}^{-1}] \quad (34)$$

We note that in both limits for a *prescribed amount of evaporation* F_{c1} scales as N_{c1}^2 so that $\Delta N = \epsilon N_{c1}$ and $x_o = N_{c2}/N_{c1}$ scale as F_{c1}/N_{c1} . Thus to get a given *small* amount of evaporation ΔN the energy flux F_c needed increases linearly with N_{c1} . This is because the higher the coronal N_{c1} , the higher the chromospheric top density n_c and the higher the radiative losses $n_c^2 f_{\text{rad}}(T)$ to be overcome by the heating $\propto n_c F_c$. To that extent our Case I loop model yields more evaporation for a *given heating flux* than Case II. On the other hand, we have seen that the initially low density Case I loop *demands more evaporation* than the high density Case II loop (by a factor of over 3) to produce a specified emission measure increase. To explain the BK data therefore Case I requires much more heating than Case II. Eq. (27) also allows us to assess what kind of spatial distribution β of heating produces the most evaporation for a given energy flux, or the minimal energy flux for a given evaporation. This is found by noting that, for given x , (26) and (27) imply $F_c \propto x^\beta/(\beta - 1)$ which minimises at $\beta = x$. This minimum

exists because if we make β large we get intense heating but only of a small mass near $N = N_c$ whereas for small β we heat a large mass but only slightly because the heating is spread out in depth. The result is also consistent with the fact that enhanced thermal conductive flux from above is not as effective as other heating mechanisms of the same total flux since conductive heating has a steep spatial gradient and corresponding loosely to a large β value.

4. Discussion and conclusions

Two issues for discussion are the physical nature of the ‘event’ heating mechanism resulting in $H_E(N)$ and the relation of ‘heating/evaporation events’ to the corona and wind as a whole. We have not specified where this heating H_E comes from, only that it declines with depth N below the transition zone. This could arise by local dissipation of energy (waves, currents) coming from below if the dissipation was most effective at lower n, N . Alternatively H_E could originate from above as waves or particles produced by magnetic energy release in the corona (micro- or nano-flares). Such coronal energy release would also involve some degree of local (coronal) heating and affect the coronal loop peak temperature attained. The temperature of the observed coronal event will be in part determined by heating of material already there and in part by arrival of hot evaporated material. If we neglect radiative and conductive cooling of this evaporating material during the evaporation event we theoretically expect it to rise in temperature by

$$\Delta T \approx F_c/(3nk\Delta N_c) \approx 0.3 \times 10^6 \text{ K} \frac{F_{c7}}{\Delta N_{c17}} \quad (35)$$

(where $F_{c7} = F_c/(10^7)$ etc.). This is of the order of or larger than the ΔT s we inferred for Cases I and II. A more detailed calculation of the ΔT expected to result from F_c in each case allowing for cooling processes, and comparison with data, may be able to give an indication of any additional direct heating of material in the corona.

We have seen that conduction alone is quite insufficient to provide the energy flux needed to drive the evaporation observed at event peak and a crucial question is the nature of the dominant heating flux - waves, particles etc. For example, the energy flux in Alfvén waves of amplitude $\delta B = bB_o$ on a field B_o carry an energy flux

$$F_{\text{Alfvén}} \approx bB_o^3/[(4\pi)^{3/2}\rho^{1/2}] \\ \approx 5 \times 10^7 \text{ erg cm}^{-2} \text{ s}^{-1} \times (10^3 b)B_{50}^3/n_{o9}^{1/2} \quad (36)$$

so that an amplitude $\delta B/B_o \approx 10^{-3}$ would carry enough flux to drive event evaporation if the waves could be deposited locally enough in the upper chromosphere.

If H_E does have its origin in nonthermal particles it is natural to ask whether there should be any detectable direct radiation signature from them - Hard X-Ray (HXR) bremsstrahlung and gyrosynchrotron radio in the case of electrons. For the single BK event our lowest evaporation model estimate of the peak energy flux over the event area A corresponds to a power

$AF_c \approx 3 \times 10^{24} \text{ erg s}^{-1}$ which is about 10^{-5} of the power in a very large flare. If we simply scale HXR fluxes by the same factor we would expect a single BK event heated by deka-keV electrons to produce a count rate in the SMM HXRBS instrument of only about 1 ct s^{-1} above 20 keV which is well below detectability. There are, however, many evaporation events on the visible solar disk at any one time - estimated by BK as several hundred, though mostly much smaller than the specific BK event analysed above. If all of these were equivalent to say 300 ‘small’ events of mean power 10% of a large one then we might expect a HRXBS count rate of 30 ct s^{-1} which should be detectable even as a quasi-steady signal. Values for the Case II interpretation would be a factor of 10 higher, which would certainly rule it out. However, small events tend to have softer HXR spectra than large ones (e.g. Hoyng et al. 1976), so that we are probably overestimating the HXRBS flux here - a conclusion consistent with the fact that in a correlation diagram of SXR versus radio event flux (Krucker & Benz 2000), small events were radio weak by more than one order, suggesting less acceleration and/or steeper electron spectra. Furthermore heating of the upper chromosphere only requires electrons of rather low energy. Ideally to test the particle driven model for evaporation events we would really like simultaneous imaged data on the HXR emission and the evaporation events themselves. Clearly the spatial, temporal, and spectral resolution of the HESSI Mission, and its low energy HXR coverage, should shed much light on these issues, especially if combined with SoHO data such as discussed here.

As far as the global relevance of micro-events is concerned, we note that 300 events of 10% of the power of the BK event we have analysed correspond to a total power of around $3 \times 10^{25-26} \text{ erg s}^{-1}$ (depending on the loop model) which is 0.5–1.5 orders down on other estimates of the total power involved in sustaining the corona. This is perhaps no surprise since we are really considering micro-events as sources of *mass* for the corona, but energetically driven by energy input from the corona itself, rather than as the source of coronal heating. As far as mass supply is concerned, on the basis of our modelling, if BK size events occurred at a rate $\nu \approx 1 \text{ s}^{-1}$ on the visible disk the over the whole sun the event mass supply rate would be (depending on the loop model) $\dot{M} \approx 2\nu\Delta\mathcal{M} \approx (0.5-1.5) \times 10^{12} \text{ g s}^{-1}$, close to that lost in the solar wind. In practice the mass supply issue is complicated by the fact that evaporated material in closed loop events will cool and fall back while events in open loops with direct access to the wind will escape, be less dense, and harder to detect. This fascinating issue is related to the preponderance of red over blue shifts in spectral line data, as discussed by e.g. Brekke et al. (1997). Indeed the preponderance of red shifts in transition region lines is so strong as to imply emptying of the corona in minutes if there were no upward motions. Inclusion of the mass flow implications of a hydrodynamic extension of our hydrostatic treatment is clearly a crucial next step forward in understanding the role of evaporative events in coronal supply.

Overall we conclude from the data presented that if the coronal mass is to be regarded as the product of transient chromospheric evaporation events then these events cannot be mainly

the result of conductively driven evaporation arising from coronal heating events. Rather coronal mass supply via transient events requires a mechanism (such as waves or particles) which heats the upper chromosphere directly, with direct coronal heating a secondary process.

Acknowledgements. This work was supported by UK PPARC Research and Travel Grants and by Visitor funds from ETH Institut für Astronomie, Zürich

References

- Antiochos S., Sturrock P.A., 1978, *ApJ* 220, 1137
 Aschwanden M.J., Nightingale R., Tarbell T.S., Wolfson C.J., 2000a, *ApJ* 535, 1027
 Aschwanden M.J., Tarbell T.D., Nightingale R.W., et al., 2000b, *ApJ* 535, 1047
 Basri G.S., Linsky J.L., Bartoe J.D., Brueckner G.E., van Hooser M.E., 1978, *ApJ* 230, 94
 Beliën A.J.C., Martens P.C.H., Keppens R., 1999, *ApJ* 526, 478
 Benz A.O., Krucker S., 1998, *Solar Physics* 182, 349
 Benz A.O., Krucker S., 1999, *A&A* 341, 286
 Berghmans D., Clette F., Moses D., 1999, *A&A* 336, 1039
 Brekke P., Hassler D.M., Wilhelm K., 1997, *Solar Phys.* 175, 349
 Brown J.C., 1973, *Solar Phys.* 31, 143
 Cox D.P., Tucker W.H., 1969, *ApJ* 157, 1157
 Craig I.J.D., McClymont A.N., 1978, *ApJ* 307, 367
 Crosby N.B., Aschwanden M.J., Dennis B.R., 1993, *Solar Phys.* 143, 275
 Fleck B., Noci G., Poletto G. (eds.), 1994, *Mass Supplies and Flows in the Solar Corona* (from *Space Sci Rev.* 70, vols. 1&2). Dordrecht: Kluwer
 Fontenla J.M., Avrett E.H., Loeser R., 1991, *ApJ* 377, 712
 Gold T., 1964, in: Hess W.N. (ed.), *AAS-NASA Symp. in the Phys. of Solar Flares*, NASA-SP 50, Washington DC, p.389
 Golub L., Pasachoff J.M., 1997, *The Solar Corona*, Cambridge: UP
 Heyvaerts J., Priest E.R., 1984, *A&A* 137, 63
 Hirth W., Krueger A., 2000, *A&A* 354, 365
 Hoyng P., van Beek H.F., Brown J.C., 1976, *Solar Phys.* 48, 197
 Hudson H.S., 1972, *Solar Phys.* 24, 414
 Ionson J., 1984, *ApJ* 276, 357
 Krucker S., Benz A.O., 1998, *ApJ* 501, L213
 Krucker S., Benz A.O., 2000, *Solar Phys.* 191, 343
 Krucker S., Benz A.O., Bastian T.S., Acton L.W., 1997, *ApJ* 488, 499
 Matthaeus W.H., Zank G.P., Oughton S., Mullan D.J., Dmitruk P., 1999, *ApJ* 523, L93
 Parker E.N., 1983, *ApJ* 264, 635
 Parker E.N., 1988, *ApJ* 330, 474
 Parnell C.E., Jupp P.E., 2000, *ApJ*, 529, 554
 Priest E.R., 1981, *Solar Flare Magnetodynamics*. London: Gordon & Breach
 Rosner R., Tucker W.H., Vaiana G.S., 1978, *ApJ* 220, 643
 Schrijver C.J., Title A.M., Berger T.E., et al., 1999, *Solar Phys.* 187, 261
 Shimizu T., Tsuneta S., Acton L.W., et al., 1994, *ApJ* 422, 906
 Shmeleva O.P., Syrovatskii S.I., 1973, *Solar Phys.* 33, 341
 Sweet P.A., 1969, *ARA&A* 7, 149
 Title A.M., Schrijver C.J., 1999, in: Donahue R.A., Bookbinder J.A. (eds.), *ASP Conf. Ser.* 154, *The Tenth Cambridge Workshop on Cool Stars, Stellar Systems and the Sun*, p. 345
 Ulmschneider P., Priest E.R., Rosner R. (eds), 1991, *Mechanisms of Chromospheric and Coronal Heating*, Springer-Verlag